Local SAR in parallel transmission pulse design

Citation: Lee, Joonsung, Matthias Gebhardt, Lawrence L. Wald, and Elfar Adalsteinsson. "Local SAR in Parallel Transmission Pulse Design." Magnetic Resonance Medicine 67, no. 6 (June 2012): 1566–1578.

As Published: http://dx.doi.org/10.1002/mrm.23140

Publisher: Wiley Blackwell

Persistent URL: http://hdl.handle.net/1721.1/85878

Version: Author's final manuscript: final author's manuscript post peer review, without publisher's formatting or copy editing

Published in final edited form as:
Magn Reson Med. 2012 June ; 67(6): 1566–1578. doi:10.1002/mrm.23140.

Local SAR in Parallel Transmission Pulse Design

Joonsung Lee[1], **Matthias Gebhardt**[2], **Lawrence L. Wald**[3,4], and **Elfar Adalsteinsson**[1,4]

[1]Department of Electrical engineering and computer science, Massachusetts Institute of Technology, Cambridge, MA 02139, United States

[2]Siemens Healthcare, Erlangen, Germany

[3]Department of Radiology, A. A. Martinos Center for Biomedical Imaging, Charlestown, MA 02129, United States

[4]Harvard-MIT Health Sciences and Technology, Massachusetts Institute of Technology, Cambridge, MA 02139, United States

Abstract

The management of local and global power deposition in human subjects (Specific Absorption Rate, SAR) is a fundamental constraint to the application of parallel transmission (pTx) systems. Even though the pTx and single channel have to meet the same SAR requirements, the complex behavior of the spatial distribution of local SAR for transmission arrays poses problems that are not encountered in conventional single-channel systems and places additional requirements on pTx RF pulse design. We propose a pTx pulse design method which builds on recent work to capture the spatial distribution of local SAR in numerical tissue models in a compressed parameterization in order to incorporate local SAR constraints within computation times that accommodate pTx pulse design during an in vivo MRI scan. Additionally, the algorithm yields a Protocol-specific Ultimate Peak in Local SAR (PUPiL SAR), which is shown to bound the achievable peak local SAR for a given excitation profile fidelity. The performance of the approach was demonstrated using a numerical human head model and a 7T eight-channel transmit array. The method reduced peak local 10g SAR by 14–66% for slice-selective pTx excitations and 2D selective pTx excitations compared to a pTx pulse design constrained only by global SAR. The primary tradeoff incurred for reducing peak local SAR was an increase in global SAR, up to 34% for the evaluated examples, which is favorable in cases where local SAR constraints dominate the pulse applications.

Keywords

Local SAR; pTx RF Design; Parallel Transmission

Introduction

Recent work has demonstrated great utility of parallel transmission (pTx) systems for radio frequency (RF) pulses in magnetic resonance imaging (MRI) for the purpose of generating more flexible magnetization profiles than is feasible with conventional single-channel RF systems (1–9). A strong motivation for the deployment of pTx RF systems is at ultra high field, such as 7 T, where pTx RF excitation benefits have been demonstrated by very effective mitigation of B1+ field inhomogeneities to achieve uniform slice selective

Corresponding Author: Joonsung Lee, Address: 77 Massachusetts Ave., Room 36-776A, Cambridge, MA 02139, USA, Telephone number: (+82) 10-6633-8417, Fax number: (+1) 617-324-3644, goplusplus@gmail.com.

excitations and spatially tailored excitations. Although pTx is an excellent tool to achieve demanding flip-angle targets, a critical challenge to routine in vivo application of this technology is the management of the specific absorption rate (SAR), which is a measure of the deposited power per unit mass of tissue due to the RF pulses. Maximum allowable values for SAR are specified by FDA and IEC guidelines (10–12) and must be met both globally, such as for power absorbed by the whole head or whole body, and locally, e.g. power absorbed per 10g of tissue. Recently, several approaches were proposed to estimate the distribution of local SAR in living subjects via B1 mapping under several assumptions that the longitudinal component of magnetic field is negligible and the variations of tissue conductivity is smaller than the variations of electric fields along integration path (13), or the axial-component of the electric field is dominant (14). Conventional approaches rely on numerical models of human anatomy and RF coils to estimate the electric field distribution due to a given pTx RF pulse, which, when combined with tissue conductivity and density can be used to generate maps of local SAR (15–17). Given such a local SAR distribution, it is straightforward to extend many of the proposed parallel RF transmission designs to incorporate penalties for local SAR in iterative optimization schemes, but the resulting computational demands are prohibitive for body models with ~mm resolution and three-dimensional field-of-view (FOV), which can yield voxel counts on the order of $\sim 10^5$–10^6.

Several pTx RF pulse design approaches have been proposed to incorporate SAR penalty in addition to the constraints on the pulse excitation performance, including the RF pulse power (4–6,18–23), which carries minimal computation penalty but naturally imposes no specific minimization of local SAR; the inclusion of global SAR penalty term (9), which incorporates measurements of forward and reflected power (24) but still does not directly penalize local SAR; multiple constraints on peak RF power, average RF power, and average SAR over multiple compartments (25) where peak local SAR over 10g tissue is not directly penalized; a so-called K maximum SAR constraints (26,27) where in an iterative scheme the design penalizes K current local SAR hotspots; and channel-dependent iterative power regularization (28), which is an iterative method to update weighting factors for excitation channels near a current hotspot. These methods can be useful to reduce both the global SAR and peak local SAR; however, they do not reveal any knowledge on the minimum peak local SAR subject to the given constraints on the pulse excitation performance and how close their peak local SAR of the pTx RF pulse to the minimum.

In this work, we describe and demonstrate a pTx RF design that incorporates electric fields from numerical simulations on human body models to jointly arrive at both a local-SAR penalized pTx pulse for a specified excitation performance fidelity, as well as a well-defined lower-bound on peak local SAR for all pTx pulses subject to the same excitation performance constraints when played on the same array for the same subject, which we refer to as the Protocol-specific Ultimate Peak in Local SAR, or the PUPiL SAR. Comparison of the local SAR achieved by an actual pulse design algorithm to the PUPiL SAR calculated for the spatial fidelity achieved provides a useful metric of the pulse design algorithm. While perhaps not needed for robust convex optimization schemes which can be counted on to find the global minimum, we propose that the PUPiL SAR value may be useful for monitoring non-convex optimization algorithms.

The local SAR minimization is general in the sense that many different and previously proposed pTx design methods are amenable to the inclusion of this power penalty and estimation of peak local SAR bounds. We demonstrate our method for three particular pTx design algorithms, RF shimming (20,29,30), spoke design (6,31,32), and arbitrary excitation for spiral trajectory (2,5,7,23,33), but the same peak local SAR constraints can be applied to e.g. spatially selective excitation (2,24), composite pTx pulses for uniform volume

excitation (21), spatial-domain design for small-flip-angle approximation (23), linear class of large-tip-angle pulses (19), and methods based on optimal control (18,22).

Our work builds on a critical development by Gebhardt et al. (34) and Eichfelder et al. (35) that decreases the complexity of the prediction of the peak local SAR in a numerical human model through the use of so-called virtual observation points, or VOPs. The VOPs effectively enable a model compression, where a model-wide peak local SAR value can be estimated to within a specified tolerance, by monitoring the virtual observation points instead of searching exhaustively over all voxels in the 3D model. We generalize the VOP model compression method for local SAR estimation to capture more dependencies among the voxels in the model and decrease the number of VOPs required to estimate local SAR. We propose a heuristic, greedy algorithm that generates VOPs to determine both lower and upper bounds on the peak local SAR for all voxels in the numerical model. The VOPs can be pre-computed once for a given model and array configuration and applied in subsequent computations to efficiently estimate peak local SAR due to a given pTx RF pulse. By capturing peaks in the local SAR distribution with VOPs, it becomes feasible to incorporate peak local SAR constraints in pTx RF designs.

Our proposed algorithm for local-SAR penalized pTx design is an iterative method that solves jointly for both a bound on peak local SAR and a pTx pulse that approaches this local SAR bound subject to the given constraints on the pulse excitation performance.

When compared to pTx pulses that only incorporate a global SAR penalty, we demonstrate 14–66% reduction in the peak local SAR (10g) for slice-selective pTx excitation and 2D selective pTx excitation while maintaining a fixed excitation performance. The peak local SAR of the demonstrated pTx designs approaches the estimated lower bound on achievable peak local SAR to within 2–36%. In return for improved peak local SAR performance, the principal trade-offs incurred by the proposed method are increased global SAR, which was less than 34% in our demonstrations, and an increased design computation time, but which is still feasible for in vivo applications (sub minute) for spoke-based pTx designs for B1+ inhomogeneity mitigation.

Methods

Local SAR estimation

FDTD numerical simulations using REMCOM (REMCOM Corp., State College, PA) (36) were used to simulate electrical fields and magnetic fields in the Virtual Family model, Ella, (37) for an eight-channel excitation array of loops for brain imaging at 7T (ω_0=297.2 MHz). The model includes both head and shoulder of the numerical model as shown in Figure 1, with voxel size of 3×3×3 mm^3, field of view in Right-Left (x), Anterior-Posterior (y), and Superior-Inferior (z) directions of 62×44×47 cm^3. The total number of voxels in this model was 269,024. The transmit array was modelled as copper loops with a voltage source and an associated pair of tuning and matching capacitors.

Using the FDTD simulations, each coil was tuned, matched, and decoupled by iteratively updating the values of tuning and matching capacitors. In each iteration, as an input, a broadband RF pulse, centered at 300MHz and with the bandwidth of 100MHz, was played on each coil, one coil at a time having all the coils present. The scattering matrix (S-matrix) was acquired and used to update the values of tuning and matching capacitors until the reflection coefficients, the diagonal elements of S-matrix, are at most −20dB and the voltage transfer ratios, the off-diagonal elements of S-matrix, are at most −40dB at the resonance frequency, 297.2MHz. Starting with the initial guess of the capacitor values, in each broadband simulation, we updated the values of the tuning and matching capacitors at the

coil element where the RF pulse was played to tune the element at 297.2MHz and match the coil element with 50Ω. Since the change of capacitor values at any other coil element can modify the reflection coefficient of the current coil element, we simulated several rounds of the eight simulations, where the RF pulse was played on each coil element one at a time.

Then we simulated electric and magnetic fields resulted from an RF pulse at the operating frequency for 7T. An RF pulse, sinusoid at frequency ω_0, with peak amplitude of 1V, was played eight times on each individual coil, k, in the array with 8 coils. For all the voxels inside the model, the resulting electric fields and magnetic fields are computed and stored as matrices, Q_v and B_v, with the dimensions (207×145×157×3)×8 for all 207×145×157 voxels, all three x, y, z components, and eight coils. Then, for any pTx RF pulse, $b(t)$, the resulting electric field at a voxel v can be calculated as $E_v(t) = Q_v b(t)$, where the RF pulse $b(t)$ is represented as a time-varying 8×1 vector of a complex-valued RF envelope.

With the rho mass density, ρ (Kg/m^3), and the electric conductivity, σ (S/m), of the head model, the sampling period of the RF, Δt, the duration of the RF, T_{RF}, the repetition time, TR, the duty cycle, $D=\frac{T_{RF}}{TR}$, time averaging local SAR at a voxel v can be determined as described in (15,38)

$$SAR_v=\frac{\sum_t SAR_v(t)\Delta t}{TR}=\frac{D\sum_t \frac{\sigma_v}{2\rho_v}\|E_v(t)\|^2\Delta t}{T_{RF}}=D\sum_t b(t)'S_v b(t),\ \text{where } S_v=\frac{\sigma_v\Delta t}{2\rho_v T_{RF}}Q_v'Q_v.$$

The regulatory limits on local SAR are specified for 10-gram tissue volumes in (10–12). For a 10-gram SAR calculation, we pre-calculate the set of voxels, indexed by w, that best approximates a 10-gram region around the voxel v, V_{10g}, and average the SAR in each 10-gram region,

$$SAR_{v,10g}=\frac{\sum_{v\in V_{10g}} SAR_v}{N_v}=D\sum_t b(t)'\left(\frac{\sum_{v\in V_{10g}} S_v}{N_v}\right)b(t)=D\sum_t b(t)'S_{v,10g}b(t), \quad [1]$$

where N_v is the number of voxels in the set, V_{10g}.

Global SAR can be obtained by averaging the SAR in the human model as

$$SAR_{global}=\frac{\sum_{v\in V_{all}} SAR_v}{N}=D\sum_t b(t)'\left(\frac{\sum_{v\in V_{all}} S_v}{N}\right)b(t)=D\sum_t b(t)'S_{Global}b(t), \quad [2]$$

where V_{all} is the set of the voxels in the model within the head and shoulder, and N is the number of voxels in the set V_{all}.

Generalized Model Compression Method for Local SAR Estimation

The proposed generalized model compression method reduces the complexity of the prediction of the peak local SAR given a human model, transmit array configuration and a fixed relative geometry between the model and the array. This method captures the peak local SAR of all the voxels, V_{all}, in a 3D numerical model by the peak local SAR of a subset

of the voxels, V_{sub}. Given an overestimating factor, ε_G, which determines the accuracy of the peak local SAR estimation in multiples of global SAR, we determine the set of voxels V_{sub}, called VOPs, that satisfies, for any RF pulse, $b(t)$, the following in terms of a lower bound and an upper bound called VOP condition:

$$\max_{v\in V_{sub}}\left\{\sum_t b(t)'S_{v,10g}b(t)\right\} \le \max_{v\in V_{all}}\left\{\sum_t b(t)'S_{v,10g}b(t)\right\} \le \max_{v\in V_{sub}}\left\{\sum_t b(t)'S_{v,10g}b(t)\right\}+\varepsilon_G\sum_t b(t)'S_{Global}b(t). \quad [3]$$

We note that in the original presentation of VOPs (34,35), the overestimation factor (ε_G) was expressed relative to RF power, whereas in the current formulation ε_G is a multiplier against global SAR. We chose the latter representation since the overestimating factor, ε_G, determines the accuracy conveniently in units of global SAR.

Since V_{sub} is a subset of V_{all}, the lower bound in the VOP condition (Eq. [3]) is always satisfied. To find the subset V_{sub} that satisfies the upper bound in the VOP condition (Eq. [3]), in the original model compression method (34,35) and our proposed generalized method, the definition is replaced by their sufficient and manageable conditions. In the original model compression method, each voxel in the model is upper-bounded by one VOP within the overestimating term, ε_G times the global SAR: Adapted so that the overestimation factor is in units of global SAR, for any voxel, v, in V_{all}, there exists a VOP, w, in V_{sub} that upper-bounds the local SAR in v within the overestimating term,

$$\sum_t b(t)'S_{v,10g}b(t) \le \sum_t b(t)'S_{w,10g}b(t)+\varepsilon_G\sum_t b(t)'S_{Global}b(t) \quad [4]$$

In the generalized model compression method, not upper-bounded by only one VOP, each voxel in the model is jointly upper-bounded by all the VOPs within the overestimating term: For any voxel v in V_{all}, there exists a set of voxel-dependent nonnegative coefficients $c_{w,v}$ whose sum is unity, $\sum_{w\in V_{sub}} c_{w,v}=1$ such that

$$\sum_t b(t)'S_{v,10g}b(t) \le \sum_{w\in V_{sub}} c_{w,v}\left(\sum_t b(t)'S_{w,10g}b(t)\right)+\varepsilon_G\sum_t b(t)'S_{Global}b(t). \quad [5]$$

Since the weighted average of local SARs in V_{sub} is less than or equal to the maximum of local SARs in V_{sub}, the condition (Eq. [5]) always implies the upper bound in the VOP condition (Eq. [3]) for any pTx RF pulse. The condition (Eq. [5]) and the voxel-dependent weighting factors, $c_{w,v}$, are only used to determine the subset, V_{sub}. However, the VOP condition that uses the peak local SAR over the VOPs will be used to evaluate the peak local SAR in the model and design the pTx RF pulses.

The generalized formulation extends the original VOP method. In the original method, for any voxel v, there exists one VOP which always bounds this voxel for any RF pulse. Whereas, in the generalized method, several VOPs may contribute to bound a voxel v, and which VOP will finally bound voxel v in Eq. [3] is allowed to depend on the waveform $b(t)$. The condition used in the original method (Eq. [4]) is a sufficient version of the condition in the generalized method (Eq. [5]), where, for a voxel v, the one of the coefficients $c_{w,v}$ is one while all others are zero. Thus, the generalized method captures more dependencies among the voxels in the model than in the original method of generating the subset V_{sub}. It decreases the number of voxels in V_{sub} required to estimate local SAR.

To validate the condition in Eq. [5] naively by calculating the both sides for infinite number of RF pulses is infeasible. Instead, the condition can be replaced by its identical condition in terms of matrix-inequalities (39,40):

$$S_{v,10g} \leq \sum_{w \in V_{sub}} c_{w,v} S_{w,10g} + \varepsilon_G S_{Global}, \quad [6]$$

which is true if all the eigenvalues of the matrix, $\sum_{w \in V_{sub}} c_{w,v} S_{w,10g} + \varepsilon_G S_{Global} - S_{v,10g}$, are nonnegative. Eigenvalues of matrix differences have been similarly used in (34,35).

To generate the V_{sub}, we have developed a heuristic, greedy algorithm as follows:

1. As an initialization step, we calculate the maximum eigenvalues of the SAR matrices, $S_{v,10g}$, of all the voxels in the 3D model and reorder the voxels based on the maximum eigenvalues in a descending order. The greedy search process will be done in this order. Then, to trade off the number of voxels in V_{sub} and the tightness of the bound in Eq. [3], choose an overestimation factor $\varepsilon_G > 0$.
2. In step 1, add the 1st voxel in V_{sub}.
3. In step k, consider kth voxel and check whether the voxel can be upper-bounded (Eq. [6]), by previously determined VOPs, voxels in V_{sub}. If not upper-bounded, then add the kth voxel in V_{sub}.
4. Finish when all the voxels have been considered.

In each greedy step (step k), to determine whether the kth voxel, v, can be upper-bounded or not by previously determined the VOPs, ideally, we need to evaluate all possible choices of the coefficient, $c_{w,v}$. To reduce the computation time, we developed an iterative method searching over the coefficients, $c_{w,v}$, as follows:

1. Initialize the coefficients.
2. If all the eigenvalues of the matrix, $P = \sum_{w \in V_{sub}} c_{w,v} S_{w,10g} + \varepsilon_G S_{Global} - S_{v,10g}$, are nonnegative, the voxel can be upper-bounded by previously determined VOPs.
3. If not, calculate the eigenvector, b, of P corresponding to the minimum eigenvalue. If, by vector b, the local SAR at the voxel v is greater than the maximum local SAR over the VOPs plus the overestimating term, i.e. $b' S_{v,10g} b > \max_{w \in V_{sub}} \{b' S_{w,10g} b\} + \varepsilon_G b' S_{Global} b$, the voxel v cannot be upper-bounded.
4. If any of the two conditions in step 2, 3 is not satisfied, update the coefficients, $c_{w,v}$, to make $b'Pb$ nonnegative.
5. Iterate step 2–4. If any of the two conditions in step 2, 3 is not satisfied until the number of iterations exceeds pre-selected the maximum number of iterations, we add the voxel v in V_{sub}.

After performing this algorithm, we have a subset, V_{sub}, for which Eq. [3] holds. This representation will be used to control peak local SAR in our pulse design. The overestimating factor, ε_G, trades off the complexity of the design and the tightness of the upper-bound of the maximum local SAR estimation. By decreasing ε_G, the approximation of the maximum local SAR is more accurate but the number of voxels in V_{sub} required to achieve this improved accuracy of bounds on maximum and minimum local SAR is increased.

Pulse Design Method

In the proposed method for pTx pulse design with efficient incorporation of local SAR constraints using the generalized model compression method, instead of minimizing the maximum local SAR of the entire model, we minimize its lower bound in the VOP condition, which is a tight lower bound for small overestimating factor, ε_G, and also can be equal to the maximum local SAR of the entire model if the voxel of the maximum local SAR belongs to the subset, V_{sub}, i.e. the maximum local SAR in the subset V_{sub}:

$$\max_{v \in V_{sub}} \left\{ \sum_t b(t)' S_{v,10g} b(t) \right\}. \quad [7]$$

The performance of this pTx pulse design is evaluated for pulses with a fixed excitation performance target, which we take to be the root mean square error (RMSE) relative to the desired transverse magnetization profile, m_d, inside the region of interest (ROI). The transverse magnetization, $m(b)$, by transmitting pTx RF pulse $b(t)$ is calculated using Bloch equation simulations. We note that the proposed design can be applied for excitation targets defined in either least-squares or magnitude-least-squares sense:

$$1.\ \text{Least Squares (LS):} RMSE = \left(\sum \| m_d - m(b) \|^2 / N_{ROI} \right)^{1/2}, \quad [8]$$

$$2.\ \text{Magnitude least squares (MLS):} RMSE = \left(\sum \| m_d - |m(b)| \|^2 / N_{ROI} \right)^{1/2}, \quad [9]$$

where N_{ROI} is the number of voxels in the region of interest.

Our iterative pTx pulse design determines the lower bound, SAR_{low}, of the peak local SAR in the subset V_{sub} we can achieve with the fixed RMSE and finds the pTx RF pulse, $b(t)$, to reach the lower bound we have determined:

$$SAR_{low} \leq \min_{RMSE=c} \left(\max_{v \in V_{sub}} \left\{ \sum_t b(t)' S_{v,10g} b(t) \right\} \right). \quad [10]$$

In our design, we only consider pTx RF pulses that minimize the weighted average of the local SAR. Among the pTx RF pulses designed, we determine the lower bound of the peak local SAR over VOPs and a pTx RF pulse that minimizes the peak local SAR over VOPs. Given nonnegative weighting factors, w_v, whose sum is equal to one, let $b_w(t)$ be a pTx RF pulse, with a fixed RMSE performance, c, that minimizes the weighted average of the local SAR:

$$b_w(t) \equiv \arg\min_{b(t)} \left\{ \sum_t b(t)' \left(\sum_{v \in V_{sub}} w_v S_{v,10g} \right) b(t) \right\} \text{ such that RMSE} = c. \quad [11]$$

The minimum weighted average of the local SAR, SAR_w, achieved by $b_w(t)$, is in fact lower than the minimum peak local SAR we can achieve.

$$SAR_w \equiv \sum_t b_w(t)' \left(\sum_{v \in V_{sub}} w_v S_{v,10g} \right) b_w(t) \le \min_{RMSE=c} \left(\max_{v \in V_{sub}} \left\{ \sum_t b(t)' S_{v,10g} b(t) \right\} \right). \quad [12]$$

The proof is as follows: Let the $b_p(t)$ be the RF pulse that minimizes peak local SAR in the subset V_{sub}, which is the first equality in Eq. [13]. The minimum peak local SAR is larger than the weighted average of the local SAR by $b_p(t)$, the first inequality in Eq. [13], since the weighting factors are nonnegative and their sum is one. The weighted average of the SAR by $b_p(t)$ is larger than the average of the local SAR by the pulse $b_w(t)$, the second inequality in Eq. [13], since we have minimized the weighted average of the local SAR. Therefore, for any nonnegative weighting factors whose sum is equal to one, the weighted average of the local SAR, SAR_w, is a lower bound on the minimum peak local SAR we can achieve..

$$\min_{RMSE=c} \left(\max_{v \in V_{sub}} \left\{ \sum_t b(t)' S_{v,10g} b(t) \right\} \right) = \max_{v \in V_{sub}} \left\{ \sum_t b_p(t)' S_{v,10g} b_p(t) \right\} \ge \sum_t b_p(t)' \left(\sum_{v \in V_{sub}} w_v S_{v,10g} \right) b_p(t) \ge \sum_t b_w(t)' \left(\sum_{v \in V_{sub}} w_v S_{v,10g} \right) b_w(t). \quad [13]$$

We define the Protocol-specific Ultimate Peak in Local SAR, or the PUPiL SAR, as the maximum, among all the weighting factors w_v, of the minimum weighted average of the local SAR, SAR_w, given V_{sub} and a fixed mitigation error:

$$PUPiL\ SAR \equiv \max_{w_v} \{SAR_w\} = \max_{w_v} \left\{ \sum_t b_w(t)' \left(\sum_{v \in V_{sub}} w_v S_{v,10g} \right) b_w(t) \right\} \text{ such that } \sum_{v \in V_{sub}} w_v = 1 \text{ and } w_v \ge 0. \quad [14]$$

We developed an iterative method to estimate the global maxima, PUPiL SAR, by searching over many weighting factors. In our initial implementation, we update weighting factors through a gradient descent method. In each iterative step, we calculate the local SAR in V_{sub} deposited by $b_w(t)$, predict the direction of the weighting factors, w_v, that increases weighting average of the local SAR and we update the weighting factors, w_v, to the direction with only a small change in each iterative step. For the initialization of the iteration, we choose equal weighting factors: $w_v = 1/N_{sub}$, where N_{sub} is the number of voxels in V_{sub}. We stop the iterative process if the weighted average of the local SAR, SAR_w, does not increase or until it reaches the preselected number of iterations.

After determining a lower bound, we then design pTx RF pulses whose peak local SAR in V_{sub} approaches the lower bound. In the previous step of determining PUPiL SAR, the goal is to find the maximum lower bound. However, the objective of our local SAR constrained pulse design is minimizing the peak local SAR in V_{sub}. In our pulse design, we still consider only the RF pulses, $b_w(t)$, that minimize the weighted average of the local SAR, but find the RF pulse that has the minimum peak local SAR in V_{sub}:

$$b(t) = \arg\min_{b_w(t)} \left(\max_{v \in V_{sub}} \left\{ \sum_t b_w(t)' S_{v,10g} b_w(t) \right\} \right), \quad [15]$$

where $b_w(t)$ satisfies Eq. [11]

We have developed an iterative method to determine the pTx RF pulse. As an initial choice to reduce the computation time, we choose as the best pTx RF pulse that has the minimum peak local SAR in V_{sub} among the pulses designed in the process of determining a lower bound. In each iterative step, we update the weighting factors, through a gradient descent method, in the direction to reduce the peak local SAR in V_{sub} and then we design the pTx RF pulse to minimize the weighted average of the local SAR. During the iterative process, the location of peak local SAR can move around. Within the accuracy of overestimation factor, the peak local SAR will nonetheless always be bounded by the VOPs, the voxels in the subset V_{sub} as shown in Eq. [3]. In our pulse design to reduce the peak local SAR over VOPs, we increase weighting factor of the peak local SAR location and constrain more so that in the next iteration, the local SAR at the peak local SAR location can be reduced. We stop the iterative process if the peak local SAR in V_{sub} does not decrease or until it reaches the preselected number of iterations.

The pTx pulse design that minimizes the weighted average of the local SAR, Eq. [11], can be implemented with a minor modification to the procedure described above for many conventional pulse design methods (5,6,18–23).

In summary, Figure 2 shows the flow diagrams that describe our proposed local SAR constrained design. To reduce the number of constraints, we perform our generalized model compression method. Then, we design pTx RF pulses to minimize the peak local SAR over the VOPs, the voxels in the subset, V_{sub}. In our method, we only design pTx RF pulses that minimize weighted averages of the local SAR and among the pTx RF pulses designed, we find the maximum weighted average of the local SAR called PUPiL SAR, which is in fact a lower bound of the peak local SAR released by the pTx RF pulse that minimizes the peak local SAR over all VOPs. Ideally, we need to consider all possible weighting factors but in our implementation we only consider several weighting factor that could represent all possible cases. The weighting factors, w_v, are the free parameters that we adjust. In each iterative step, we design one pTx RF pulse to minimize the weighted average of the local SAR with the weighting factors, w_v, calculate the local SAR over VOPs, and update weighting factors as it is shown in Figure 2b. The computation time for designing a pTx RF pulse to minimize the weighted average of the local SAR is almost the same as the computation time for designing conventional RF power constrained design, and is much larger than the time to compute local SAR over VOPs.

Results

Model Compression for Local SAR Estimation

We performed the original and the proposed generalized model compression methods for local SAR estimation for several different overestimating factors, ε_G, from 0.7 to 10. Figure 3a shows the number of voxels in V_{sub}, N_{sub}, determined by the original (blue) and the generalize (green) method. In Figure 3b, the ratio of N_{sub} in two methods to achieve a given overestimation factor is shown. The generalized approach captures local SAR estimates at an overestimation level of $\varepsilon_G = 1$ with approximately 6-fold fewer voxels (Figure 3b) than the original method. The generalized model compression method can reduce the complexity of the peak local SAR calculation for every voxel in the head and shoulder model (~10^5 voxels) to only the voxels in the subset V_{sub} (in our case, ~10^2) at an overestimation level of $\varepsilon_G = 1$. In Figure 3c, the computation time is shown for two methods, the original (blue) and the generalize (green). The generalized method took 1.4–17 times longer than the original method. For an overestimation level of $\varepsilon_G = 0.7$, the computation time of the generalized method was about a day using Matlab2010b (Mathworks, Natick, MA, USA) processed by one core of the PC (Intel Core i7–2600 CPU 5160, 3.8GHz), but this lengthy computation only has to be carried out once given a human model, transmit array configuration and a

fixed relative geometry between the model and the array. Figure 4 shows the locations of VOPs (white dots) in seven sagittal slices, which is 1.5cm apart each other. In (a–c), the VOPs from original model compression method are shown at $\varepsilon_G = 1, 2, 3$. In (d–e), the VOPs from generalized model compression method are shown at $\varepsilon_G = 1, 2, 3$. Compared to the original model compression method, the number of VOPs is greatly reduced in the generalized model compression method.

Pulse Design with local SAR constraints

We demonstrate the application of the local SAR reduction in pTx design by designing pTx pulses for two different low-flip-angle applications. The first is to mitigate B1+ magnitude inhomogeneity in the Ella head model at 7T for an axial, 1-cm thick, slice-selective excitation at the S-I center of the RF coil array, while the second design uses a spiral-based excitation k-space trajectory with a square-box target pattern of uniform intensity in dimensions of $x \times y = 63 \times 63$ mm^2, with zero excitation outside the box. The desired profiles (Figure 5) are chosen to have the maximum normalized transverse magnetization of 0.5 (equivalent to a 30° flip angle) assuming that the fully relaxed longitudinal magnetization is unity. For the slice-selective application, we considered three different design categories for pTx pulses, namely RF shimming with an MLS criterion, a two-spoke pulse with the MLS criterion (6), and a four-spoke pulse with the LS criterion. For the box excitation, we used a 2D spiral pTx pulse (5) with the MLS criterion with an acceleration factor of four and FOV of 27cm in x and y, and resolution of 3mm. For this demonstration, the simulated B1+ fields were used and B0 was assumed to be homogenous. For these simulations, the duty cycle was assumed to be 100%, i.e. TR equals the duration of the RF pulse. The durations of RF pulses are 1.6ms for MLS RF Shimming, 2.51ms for MLS two spokes, 4.16ms for LS four spokes, and 5.95ms for 2D spiral pTx pulse.

While we constrained the peak local SAR of the voxels in the subset V_{sub} generated by the generalized model compression method at an overestimation level of $\varepsilon_G = 1$ in the proposed design, to evaluate the performance, the peak 10g local SAR over the entire model was calculated by performing an exhaustive search. The performance of the proposed method was compared to pTx pulses designed without an explicit local-SAR penalty, but rather with constraints on either a total pulse power (5,6,20) or global SAR (9),

1. Power constrained: $b(t) = \arg\min_{b(t)} \left(\sum_t b(t)' b(t) \right)$ such that RMSE = c,
2. Global SAR constrained: $b(t) = \arg\min_{b(t)} \left(\sum_t b(t)' S_{Global} b(t) \right)$ such that RMSE = c.

For all our calculation of the pTx RF pulses to satisfy the fixed RMSE, we regard the SAR constraints, weighted average of the local SAR in the proposed method, RF power in the power constrained method, and global SAR in the global SAR constrained methods a regularization term, i.e. $b(t) = \arg\min_{b(t)} (RMSE + \lambda SAR)$. We then design with several values of regularization parameter, λ, and find the pTx RF pulse that satisfy the desired excitation performance, a fixed RMSE.

In Figure 6, the peak local SAR over the entire model is shown: a lower bound (the estimate of the PUPiL SAR, blue), proposed local SAR constrained design (green), an upper bound (the overestimation of the peak local SAR determined by VOPs in Eq. [3], cyan), global SAR constrained design (black), and RF power constrained design (red). For all the cases, the peak local SAR of the proposed method (green) is larger than the lower bound (blue) and is less than the upper bound (cyan). The reduction of the peak local SAR varies with the

pulse design method. The ratio of the peak local SAR of proposed local SAR constrained design to the peak local SAR of global SAR constrained design (green/black) was 64–86% for MLS RF Shimming, 53–72% for MLS two spokes, 60–85% for LS four spokes, and 34–48% for MLS 2D spiral. The ratio of the peak local SAR of proposed local SAR constrained design to the lower bound was 102–109% for MLS RF Shimming, 106–135% for MLS two spokes, 104–119% for LS four spokes, and 112–136% for MLS 2D spiral. The ratio of the peak local SAR of proposed local SAR constrained design to the upper bound was 87–90% for MLS RF Shimming, 83–86% for MLS two spokes, 83–89% for LS four spokes, and 81–85% for MLS 2D spiral.

For MLS two spokes, LS four spokes, and MLS 2D spiral designs, the peak local SAR of the RF power constrained design was larger than the peak local SAR of the global SAR constrained. However, for MLS RF Shimming, the peak local SAR of the RF power constrained design was smaller than the peak local SAR of the global SAR constrained. Global SAR constraint design only guarantees that the global SAR is minimized, but it does not guarantee that peak local SAR is minimized. Infinite number of RF pulses with the same excitation fidelity may exist that have a lower peak local SAR. One example is local SAR constrained design. For our case of MLS RF Shimming, RF power constrained design happened to have the lower peak local SAR. Also, we found that even with the large mitigation error, it is possible to have larger peak local SAR for global SAR constrained design and RF power constrained design.

For B1+ mitigation of slice-selective excitation with 30 flip angle, at RMSE = 0.08, the minimum TR required not to violate the FDA limit on the peak local SAR, 10 W/Kg over any 10g tissue, is 6.3 ms (1.6 ms) for MLS RF Shimming, 1.73 ms (2.51 ms) for MLS two spokes, and 1.74 ms (4.16 ms) for LS four spokes.

One of the trade-offs in the proposed method is an increased global SAR. As it is shown in Figure 7, compared to the global SAR constrained design, the global SAR was 110–117% for MLS RF Shimming, 109–119% for MLS two spokes, 106–132% for LS four spokes, and 119–134% for MLS 2D spiral for box excitation. The other trade-off is the increased computation time due to the iterative procedure. The number of iterations in the proposed method was 14–31 for MLS RF Shimming, 23–45 for MLS two spokes, 24–32 for LS four spokes, and 50 for MLS 2D spiral.

Figure 8 shows the distribution of 10g local SAR corresponding to the 2D spiral design corresponding with the mitigation error of RMSE = 0.025. In Figure 8a, the 10g local SAR maps, the sagittal, coronal, and axial slices containing the voxel with the peak 10g local SAR in the entire model, as identified by an exhaustive search, are shown. The peak 10g local SAR is decreased by 54% compared to the global SAR constrained design and 63% compared to the power constrained design. The hottest voxel is in a different location in the local SAR constrained pTx RF design method than in the global SAR constrained design and RF power constrained design. In Figure 8b, the 10g local SAR of the entire 3D voxels is shown in a descending order for the proposed method (green) and the global SAR constrained method (black). Compared to the global SAR constrained method, the peak local SAR is reduced by trading off the local SAR of other voxels and the global SAR.

Discussion

We proposed an iterative pTx pulse design method which incorporates constraints on peak local SAR for a given human model and transmit array configuration. A weighted average of local SAR, which is a lower bound of the peak local SAR, is minimized in each iterative step of the pTx design. The proposed method also determines a lower bound on the peak

local SAR, PUPiL SAR, and the pTx RF pulse closest to the lower bound while still satisfying the given excitation performance criterion.

While we demonstrated the utility of our approach with pTx pulses designed by RF shimming (20,29,30), magnitude least square spoke design (6), least-squares spoke design, and arbitrary excitation for spiral trajectory (2,5,7,23,33), the method is general in that it extends to and is compatible with other pTx pulse design methods such as spatially selective excitation (2,24), composite pTx pulse for uniform volume excitation (21), spatial domain design for small flip angle approximation (23), LCLTA (19), and optimal control approaches (18,22).

In a numerical head model, we demonstrated 14–66% of reduction in the peak local 10g SAR for slice-selective pTx excitation and 2D selective pTx excitation compared to the global SAR constrained design. The trade-offs of the proposed method are increased global SAR, within 34% in our demonstrations, and increased computation time by a factor of 14–50.

In Figure 9, the peak local SAR over the entire model (green) and its upper bound (Eq. [3]), which is the peak local SAR of the voxels in the subset, V_{sub}, determined by the model compression method plus the overestimation term (cyan), are shown for $\varepsilon_G = 1$–9 and four pTx RF designs. For small overestimating factor, $\varepsilon_G = 1$, the peak local SAR is 82~89% of its upper bound in Eq. [3]. However, for large overestimating factor, $\varepsilon_G = 9$, the peak local SAR is 42~48% of its upper bound.

The peak local SAR of the pTx pulses exceeds the PUPiL SAR by 2–36%. In Figure 10, the peak local SAR over the entire model (green), the peak local SAR of the voxels in the subset V_{sub} determined by the model compression method (black), and a lower bound (the estimate of the PUPiL SAR, blue), are shown for $\varepsilon_G = 1$–9 and four pTx RF designs. As it is shown in Figure 9 and 10, for our local SAR constrained pulse design, the peak local SAR over the entire model is much closer to the lower bound than its upper bound in Eq. [3]. The gap between the peak local SAR over the entire model and the lower bound can be reduced in two ways. First, by using the smaller overestimating factors, which takes longer to compute VOPs and increases the number of VOPs considered in the computation of the lower bound, the difference between the peak local SAR over the entire model and the peak local SAR at the voxels in the subset V_{sub} is reduced. As a future work, we will investigate the limitation of our local SAR constrained design; how many VOPs can our method deal with and how much the number of iteration to converge increases if we use more VOPs.

Alternatively, by improving the method for updating the weighting factors or considering more combinations of weighting factors, w_v, the global maximum of weighted average of the local SAR could be determined and the gap between the peak local SAR at the voxels in the subset V_{sub} and the lower bound can be reduced. In our current implementation, which is a gradient descent method, our estimate of the PUPiL SAR may converge to a local maximum.

Our design method to minimize the peak local SAR over VOPs, voxels in the subset, V_{sub}, considers only the pTx RF pulses that minimize the weighted average of the local SAR in Eq. [11]. By doing this, we can address minimization over hundreds of peak local SAR constraints. This approach also can be applied to many conventional pulse design methods (5,6,18–23) and can be implemented with a minor modification in their implementations. The trade-off is the increased computation time, by a factor of the number of pTx RF pulses, $b_w(t)$, designed. The computation time can be reduced by parallel computing, designing several pTx RF pulses simultaneously. However, to minimize the peak local SAR further, we might need to consider all possible pTx RF pulses given excitation performance

criterion. The methods that minimize the peak local SAR using second order cone programming (25,26) may be useful. Before its use, the applicability of the methods, in terms of the number of constraints that the methods can solve and their computation time, should be investigated

The generalized VOP method and proposed pulse design method were demonstrated for a given a human model, transmit array configuration, and a fixed relative geometry between the model and the array. As a future work, we will generalize the proposed method to impose peak local SAR constraints on several configurations of human model and transmit arrays, which can differ by types of the human model or the relative geometry between the model and the array. This could jointly minimize the peak local SAR by trading off peak local SAR for one configuration compared to the optimized method for one configuration. To proceed, we need to have simulated electric fields on the several configurations.

While the proposed pulse design method is demonstrated for the design of a single pulse, it can be generalized to joint pulse design over a set of pTx pulses to further reduce the time-average peak local SAR (26,41). For instance, in pulse sequences that apply saturation pulses prior to excitation, a joint design of the saturation and excitation pulses with local-SAR penalty could yield better local-SAR performance than if each pTx pulse is designed in isolation, and further, a joint design of a family of slice-selective excitation pulses in multi-slice acquisitions could be performed to minimize peak local SAR over the duration of the multi-slice scan.

Conclusion

The incorporation of peak local SAR constraints in pTx RF design was made feasible by the model compression method for estimation of peak local SAR, which dramatically reduces the number of voxels that need to be considered. The original model compression method (34,35) was generalized to capture additional local-SAR dependencies among voxels. The proposed pTx pulse design minimizes peak local SAR while satisfying the given excitation performance target, and yields a bound on the achievable SAR performance, the PUPiL SAR.

Acknowledgments

This work is supported by Siemens Healthcare, The Siemens-MIT Alliance, National Institute of Health NIH R01EB006847, NIH R01EB007942, and NCRR P41RR14075. The authors acknowledge Lohith Kini, MEng, Berkin Bilgic, SM, Borjan Gagoski, Ph.D, Kawin Setsompop, Ph.D., and Khaldoun Makhoul, Ph.D., for help with FDTD simulations and beneficial discussions.

References

1. Alagappan V, Nistler J, Adalsteinsson E, Setsompop K, Fontius U, Zelinski A, Vester M, Wiggins GC, Hebrank F, Renz W, Schmitt F, Wald LL. Degenerate mode band-pass birdcage coil for accelerated parallel excitation. Magn Reson Med. 2007; 57(6):1148–1158. [PubMed: 17534905]
2. Katscher U, Bornert P, Leussler C, van den Brink JS. Transmit SENSE. Magn Reson Med. 2003; 49(1):144–150. [PubMed: 12509830]
3. Setsompop K, Alagappan V, Gagoski B, Witzel T, Polimeni J, Potthast A, Hebrank F, Fontius U, Schmitt F, Wald LL, Adalsteinsson E. Slice-selective RF pulses for in vivo B1+ inhomogeneity mitigation at 7 tesla using parallel RF excitation with a 16-element coil. Magn Reson Med. 2008; 60(6):1422–1432. [PubMed: 19025908]
4. Setsompop K, Alagappan V, Gagoski BA, Potthast A, Hebrank F, Fontius U, Schmitt F, Wald LL, Adalsteinsson E. Broadband slab selection with B1+ mitigation at 7T via parallel spectral-spatial excitation. Magn Reson Med. 2009; 61(2):493–500. [PubMed: 19161170]

5. Setsompop K, Wald LL, Alagappan V, Gagoski B, Hebrank F, Fontius U, Schmitt F, Adalsteinsson E. Parallel RF transmission with eight channels at 3 Tesla. Magn Reson Med. 2006; 56(5):1163–1171. [PubMed: 17036289]
6. Setsompop K, Wald LL, Alagappan V, Gagoski BA, Adalsteinsson E. Magnitude least squares optimization for parallel radio frequency excitation design demonstrated at 7 Tesla with eight channels. Magn Reson Med. 2008; 59(4):908–915. [PubMed: 18383281]
7. Ullmann P, Junge S, Wick M, Seifert F, Ruhm W, Hennig J. Experimental analysis of parallel excitation using dedicated coil setups and simultaneous RF transmission on multiple channels. Magn Reson Med. 2005; 54(4):994–1001. [PubMed: 16155886]
8. Wiggins, G.; Mareyam, A.; Setsompop, K.; Alagappan, V.; Potthast, A.; Wald, L. A Close-Fitting 7 Tesla 8 Channel Transmit/Receive Helmet Array with Dodecahedral Symmetry and B1 Variation Along Z. Proc Intl Soc Mag Reson Med.; Toronto, Canada. 2008. p. 148
9. Zhu Y. Parallel excitation with an array of transmit coils. Magn Reson Med. 2004; 51(4):775–784. [PubMed: 15065251]
10. IEC Standard 60601-2-33, Particular requirements for the safety of magnetic resonance equipment for medical diagnosis. Chicago: International Electrotechnical Commission; 2004.
11. International Electrotechnical Commission. International standard, Medical equipment—part 2: particular requirements for the safety of magnetic resonance equipment for medical diagnosis, 2nd revision. Geneva: International Electrotechnical Commission; 2002. p. 29-31.
12. Center for Devices and Radiologic Health. Guidance for the submission of premarket notifications for magnetic resonance diagnostic devices. Rockville, MD: Food and Drug Administration; 1998.
13. Voigt, T.; Doessel, O.; Katscher, U. Imaging conductivity and local SAR of the human brain. Proc Intl Soc Mag Reson Med.; Honolulu, Hawaii, USA. 2009. p. 4531
14. Cloos, MA.; Bonmassar, G. Towards Direct B1 Based Local SAR Estimation. Proc Intl Soc Mag Reson Med.; Honolulu, Hawaii, USA. 2009. p. 3037
15. Collins CM, Li S, Smith MB. SAR and B1 field distributions in a heterogeneous human head model within a birdcage coil. Specific energy absorption rate. Magn Reson Med. 1998; 40(6):847–856. [PubMed: 9840829]
16. Collins CM, Smith MB. Calculations of B1 distribution, SNR, and SAR for a surface coil adjacent to an anatomically-accurate human body model. Magnetic Resonance in Medicine. 2001; 45(4): 692–699. [PubMed: 11283998]
17. Zelinski AC, Angelone LM, Goyal VK, Bonmassar G, Adalsteinsson E, Wald LL. Specific absorption rate studies of the parallel transmission of inner-volume excitations at 7T. J Magn Reson Imaging. 2008; 28(4):1005–1018. [PubMed: 18821601]
18. Xu D, King KF, Zhu Y, McKinnon GC, Liang ZP. Designing multichannel, multidimensional, arbitrary flip angle RF pulses using an optimal control approach. Magn Reson Med. 2008; 59(3): 547–560. [PubMed: 18306407]
19. Xu D, King KF, Zhu Y, McKinnon GC, Liang ZP. A noniterative method to design large-tip-angle multidimensional spatially-selective radio frequency pulses for parallel transmission. Magn Reson Med. 2007; 58(2):326–334. [PubMed: 17654576]
20. Mao W, Smith MB, Collins CM. Exploring the limits of RF shimming for high-field MRI of the human head. Magn Reson Med. 2006; 56(4):918–922. [PubMed: 16958070]
21. Gumbrecht, R.; Lee, J.; Fautz, H-P.; Diehl, D.; E, A. Fast high-flip pTx pulse design to mitigate B1+ inhomogeneity using composite pulses at 7T. Proc Intl Soc Mag Reson Med.; Stockholm, Sweden. 2010. p. 101
22. Grissom WA, Xu D, Kerr AB, Fessler JA, Noll DC. Fast large-tip-angle multidimensional and parallel RF pulse design in MRI. IEEE Trans Med Imaging. 2009; 28(10):1548–1559. [PubMed: 19447704]
23. Grissom W, Yip CY, Zhang Z, Stenger VA, Fessler JA, Noll DC. Spatial domain method for the design of RF pulses in multicoil parallel excitation. Magn Reson Med. 2006; 56(3):620–629. [PubMed: 16894579]
24. Zhu, Y. In Vivo RF Power and SAR Calibration for Multi-Port RF Transmission. Proc Intl Soc Mag Reson Med.; Honolulu, Hawaii, USA. 2009. p. 599

25. Brunner DO, Pruessmann KP. Optimal design of multiple-channel RF pulses under strict power and SAR constraints. Magn Reson Med. 2010; 63(5):1280–1291. [PubMed: 20432299]
26. Graesslin, ISC.; Annighoefer, B.; Weller, J.; Diederer, S.; Brunner, D.; Homann, H.; Schweser, F.; Katscher, U.; Pruessmann, K.; Boernert, P. Local SAR constrained Hotspot Reduction by Temporal Averaging. Proc Intl Soc Mag Reson Med.; Stockholm, Sweden. 2010. p. 4932
27. Graesslin, I.; Schweser, F.; Annighoefer, B.; Biederer, S.; Katscher, U.; Nehrke, K.; Stahl, H.; Dingemans, H.; Mens, G.; Bornert, P. A Minimum SAR RF Pulse Design Approach for Parallel Tx with Local Hot Spot Suppression and Exact Fidelity Constraint. Proc Intl Soc Mag Reson Med.; Toronto, Canada. 2008. p. 621
28. Cloos MA, Luong M, Ferrand G, Amadon A, Le Bihan D, Boulant N. Local SAR reduction in parallel excitation based on channel-dependent Tikhonov parameters. Journal of Magnetic Resonance Imaging. 2010; 32(5):1209–1216. [PubMed: 21031527]
29. Hoult DI, Phil D. Sensitivity and power deposition in a high-field imaging experiment. J Magn Reson Imaging. 2000; 12(1):46–67. [PubMed: 10931564]
30. Ibrahim TS, Lee R, Baertlein BA, Kangarlu A, Robitaille PL. Application of finite difference time domain method for the design of birdcage RF head coils using multi-port excitations. Magn Reson Imaging. 2000; 18(6):733–742. [PubMed: 10930783]
31. Ulloa, JL.; Irarrazaval, P.; Hajnal, JV. Proc Intl Soc Mag Reson Med. Florida, USA: Miami Beach; 2005. Exploring 3D RF shimming for slice selective imaging; p. 21
32. Saekho S, Yip CY, Noll DC, Boada FE, Stenger VA. Fast-kz three-dimensional tailored radiofrequency pulse for reduced B1 inhomogeneity. Magn Reson Med. 2006; 55(4):719–724. [PubMed: 16526012]
33. Pauly J, Nishimura D, Macovski A. A K-Space Analysis of Small-Tip-Angle Excitation. J Magn Reson. 1989; 81(1):43–56.
34. Gebhardt, M.; Diehl, D.; Adalsteinsson, E.; Wald, LL.; Eichfelder, G. Evaluation of Maximum Local SAR for Parallel Transmission (PTx) Pulses Based on Pre-Calculated Field Data Using a Selected Subset of "Virtual Observation Points". Proc Intl Soc Mag Reson Med.; Stockholm, Sweden. 2010. p. 1441
35. Eichfelder G, Gebhardt M. Local specific absorption rate control for parallel transmission by virtual observation points. Magn Reson Med. 2011
36. Taflove, A.; Hagness, SC. Computational electrodynamics: the finite-difference time-domain method. Boston: Artech House; 2000. p. 852p. xxiii
37. Christ A, Kainz W, Hahn EG, Honegger K, Zefferer M, Neufeld E, Rascher W, Janka R, Bautz W, Chen J, Kiefer B, Schmitt P, Hollenbach HP, Shen JX, Oberle M, Szczerba D, Kam A, Guag JW, Kuster N. The Virtual Family-development of surface-based anatomical models of two adults and two children for dosimetric simulations. Phys Med Biol. 2010; 55(2):N23–N38. [PubMed: 20019402]
38. IEEE Recommended Practice for Measurements and Computations of Radio Frequency Electromagnetic Fields With Respect to Human Exposure to Such Fields,100 kHz-300 GHz. IEEE Std C953–2002 (Revision of IEEE Std C953–1991). 2002 i-126.
39. Strang, G. Introduction to linear algebra. Wellesley, MA: Wellesley-Cambridge Press; 2009. p. 574p. ix
40. Zhan, X. Matrix inequalities. Berlin; New York: Springer; 2002. p. 116p. vi
41. Graesslin, I.; Weller, J.; Schweser, F.; Annighoefer, B.; Diederer, S.; Katscher, U.; Nielsen, T.; Harvey, P.; Boernert, P. SAR Hotspot Reduction by Temporal Averaging in Parallel Transmission. Proc Intl Soc Mag Reson Med.; Honolulu, Hawaii, USA. 2009. p. 3037

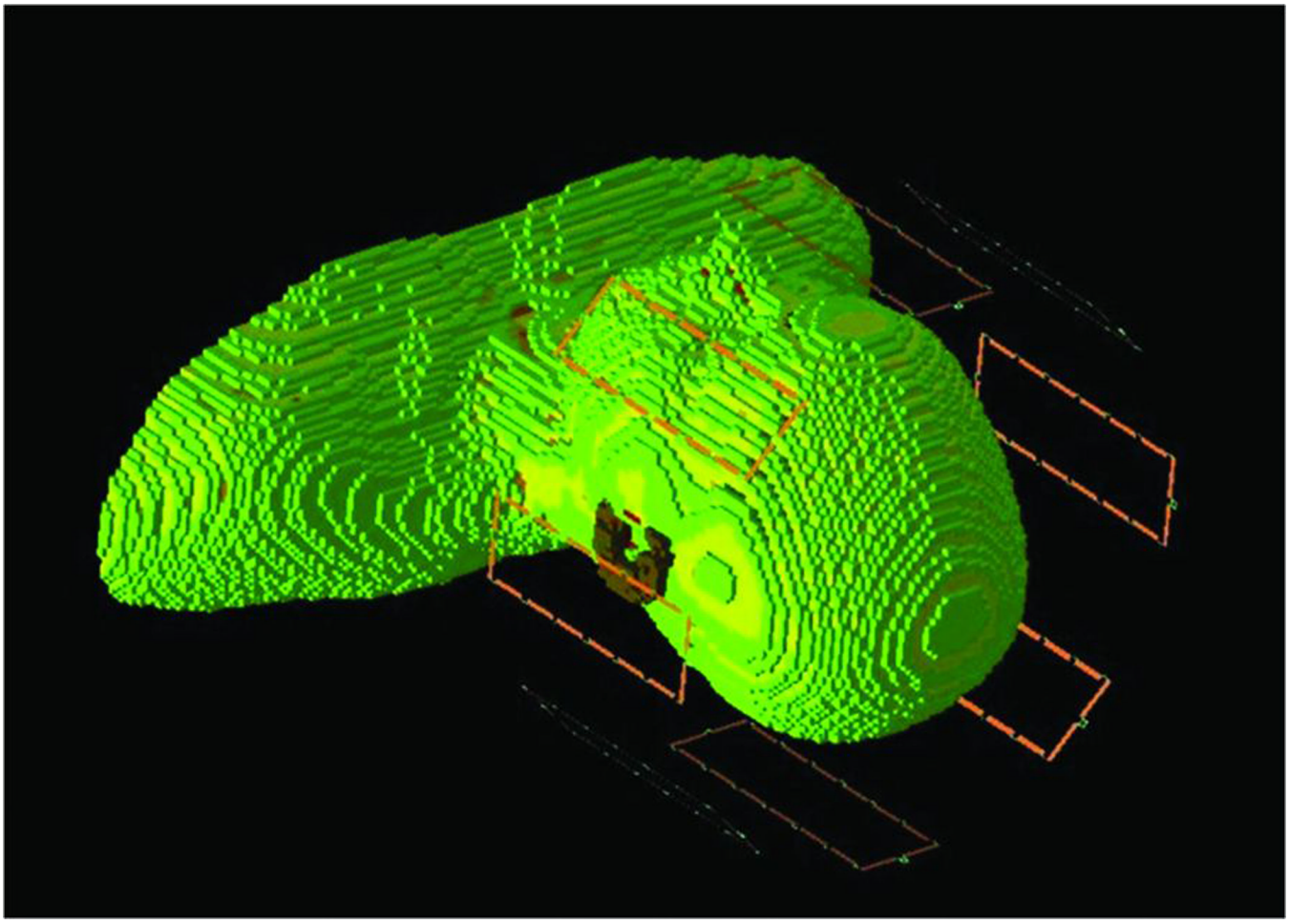

Figure 1.
Shaded-surface rendition of the 3D numerical head and shoulders model of Ella, a member of the virtual family, placed in an eight-channel excitation loop coil array.

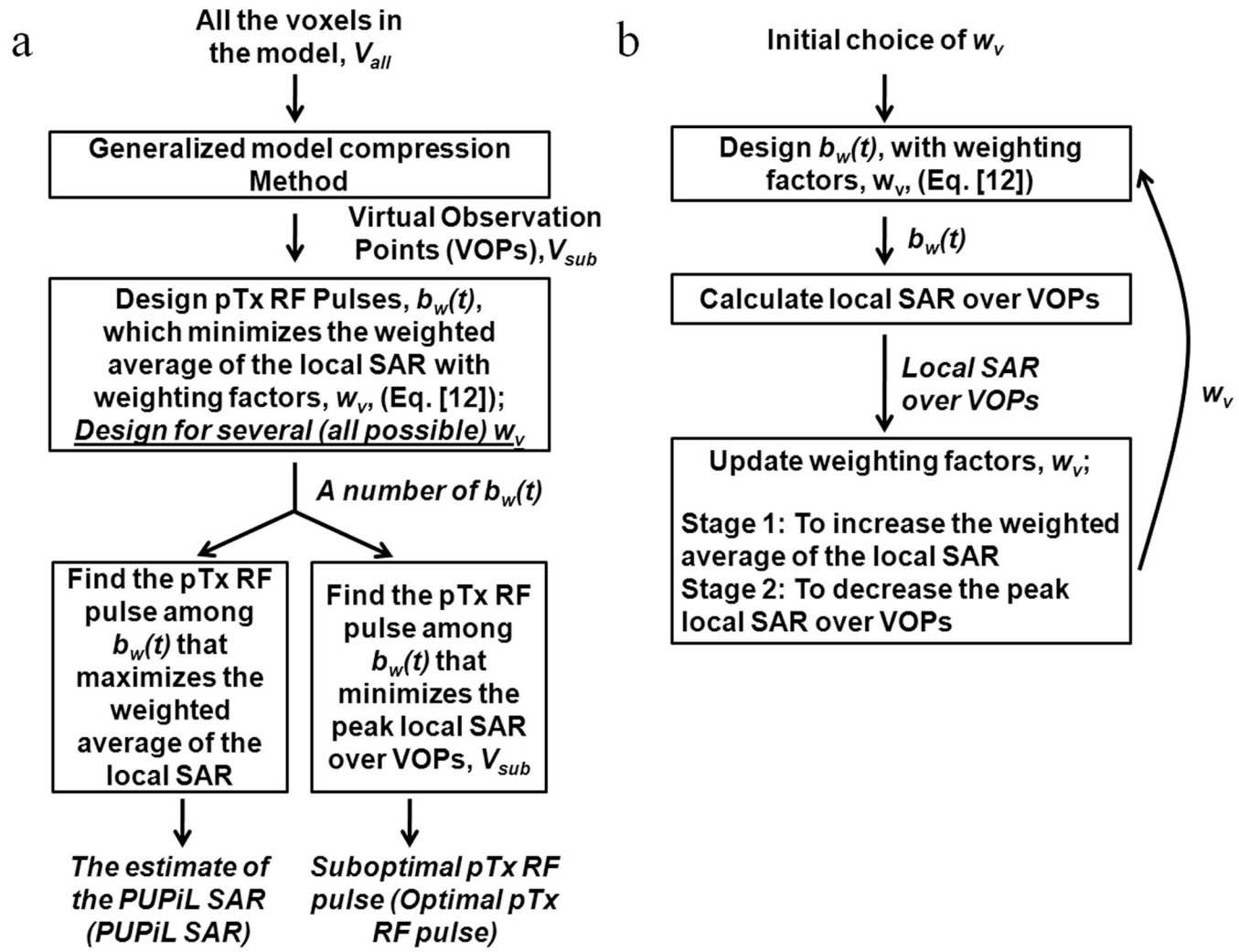

Figure 2.

(a) Flow diagram of our local SAR constrained pTx RF pulse design. Our design finds the lower bound of the peak local SAR over VOPs called PUPiL SAR, the maximum weighted average of the local SAR, and pTx pulses that minimizes the peak local SAR over VOPs among $b_w(t)$, which minimizes the weighted average of the local SAR given weighting factors. In our implementation, instead of considering all possible weighting factors, (ideal case noted as in parenthesis), we consider only several weighting factors. (b) Flow diagram of iterative method to choose weighting factors.

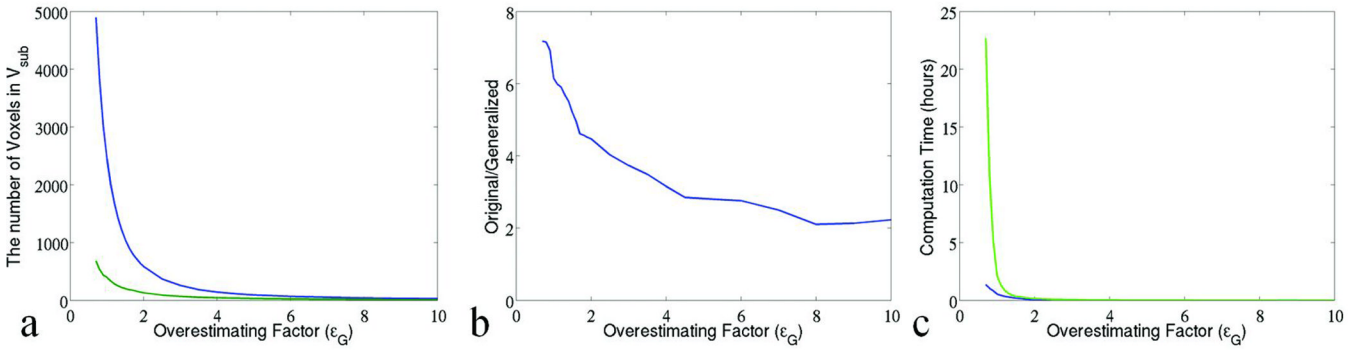

Figure 3.

(a) The number of voxels in the subset, V_{sub}, determined by model compression methods as a function of the overestimating factor, ε_G, the proposed generalized method for VOP classification is in green, whereas the original method is shown in blue. (b) The ratio of the two curves in (a), original/generalized, demonstrating up to a six-fold reduction in the number of VOPs needed to adequately capture peak local SAR for ε_G=1. (c) Computation time of two methods: Proposed generalized method (green), original method (blue).

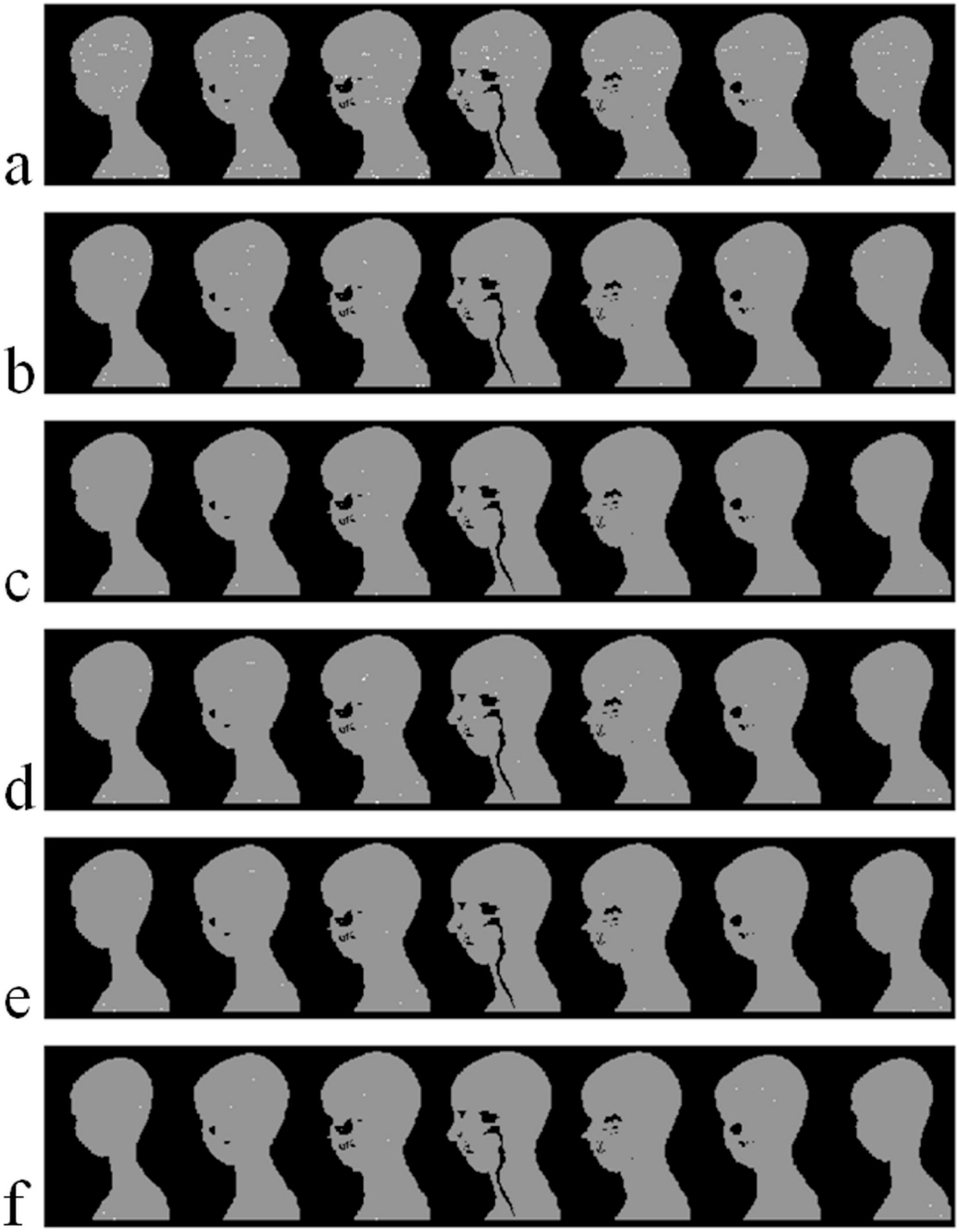

Figure 4.
The location of VOPs in seven sagittal slices, which is 1.5cm apart each other. (a) Original method at $\varepsilon_G = 1$, (b) Original method at $\varepsilon_G = 2$, (c) Original method at $\varepsilon_G = 3$, (d) Generalized method at $\varepsilon_G = 1$, (e) Generalized method at $\varepsilon_G = 2$, (f) Generalized method at $\varepsilon_G = 3$.

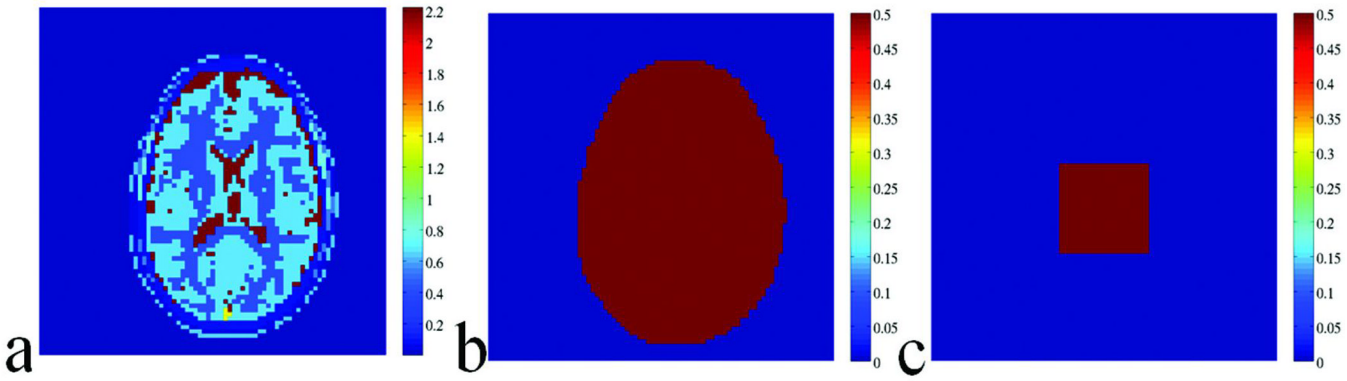

Figure 5.

(a) Axial section of conductivity map at the S-I center of the RF coil array in S/m with voxel size of 3×3×3 mm^3, Target profiles for transverse magnetization normalized to a maximum of unity within a FOV of 24cm for (b) a slice-selective, uniform flip angle for B1+ mitigation with RF shimming or spoke-based excitation, and (c) a 2D, square box excitation target for a spiral-based excitation.

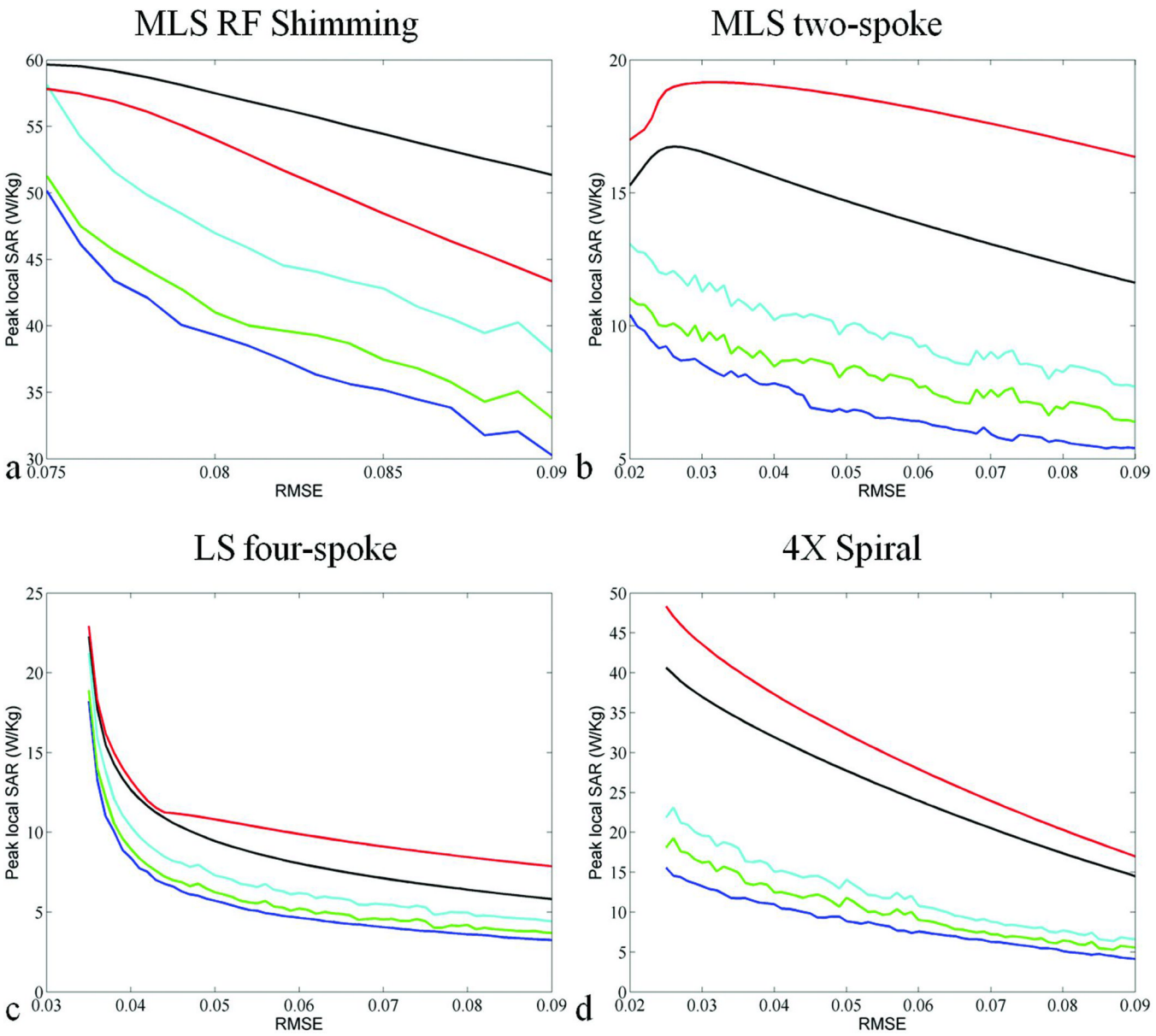

Figure 6.

Peak 10g local SAR over the entire model for pulses played with a 100% duty-cycle as a function of Root-mean-square error (RMSE) of pTx excitation performance, showing the lower bound for peak local SAR as estimated by the proposed design algorithm, the PUPiL SAR, (blue), peak local SAR of the pTx pulse design achieved by the proposed method (green), the overestimation of the peak local SAR determined by VOPs (cyan), peak local SAR incurred by pTx design that was only penalized for global SAR (black), and peak local SAR for RF power constrained design (red). These data are shown for a) magnitude-least-squares (MLS) RF shimming for slice-selective B1+ inhomogeneity mitigation, (b) MLS two-spoke pTx design for the same slice-selective target as in (a), (c) least-squares (LS), four-spoke design for the same target as in (a), and (d) a 2D spiral-based pTx excitation for a square-box excitation with a four-fold acceleration.

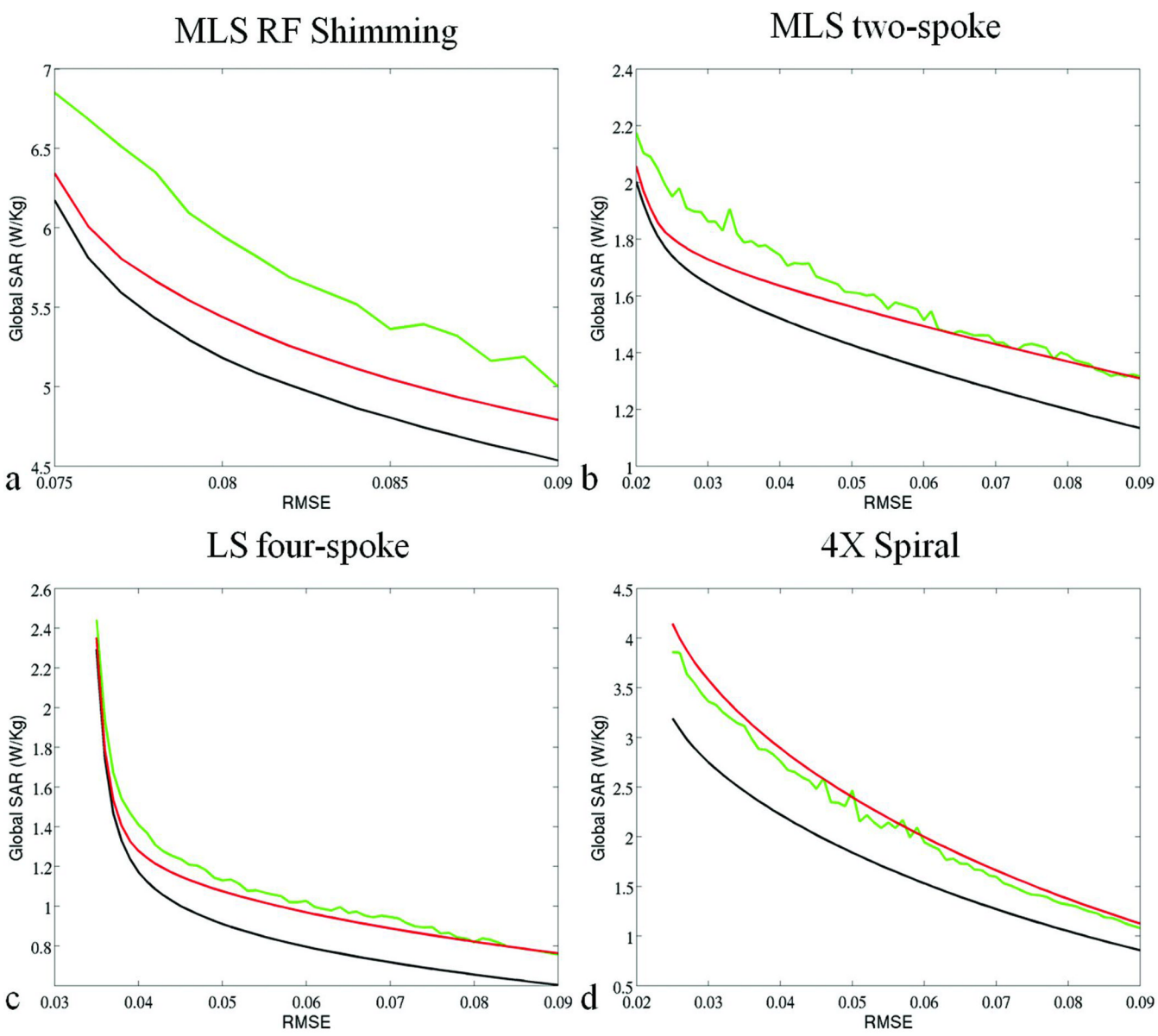

Figure 7.

Global SAR for pulses played with a 100% duty-cycle as a function of Root-mean-square error (RMSE) of pTx excitation performance. The graphs show the global SAR for the proposed pTx design method (green), a global-SAR constrained design (black), and RF-power-constrained design (red). These data are shown for (a) magnitude-least-squares (MLS) RF shimming for slice-selective B1+ inhomogeneity mitigation, (b) MLS two-spoke pTx design for the same slice-selective target as in (a), (c) least-squares (LS), four-spoke design for the same target as in (a), and (d) a 2D spiral-based pTx excitation for a square-box excitation with a four-fold acceleration.

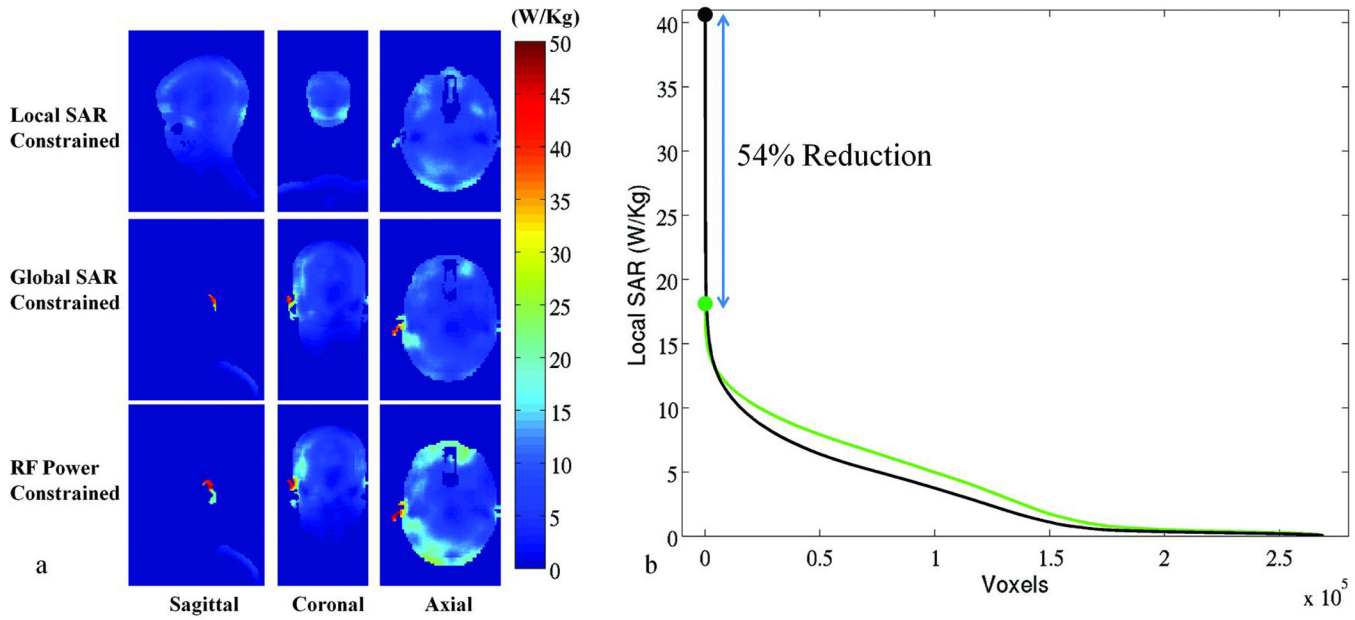

Figure 8.

The distribution of 10g local SAR corresponding to the 2D-spiral based pTx design for square-box excitation corresponding to an excitation target error, measured as root-mean-square error (RMSE) of 0.025, (a) 10g local SAR maps of sagittal, coronal, and axial slices containing the voxel with the peak 10g local SAR for the proposed method (top row), which achieved 54% decrease of the peak local SAR compared to the global-SAR-constrained design (middle row) and 63% decrease of the peak local SAR compared to the RF-power-constrained design (bottom row). In panel (b), the graph displays 10g local SAR of the entire set of voxels in the model, sorted in descending order, with the proposed local-SAR constrained design method in green, and the global-SAR-constrained method in black, demonstrating both the substantial decrease in peak local SAR (dramatic drop from black to green curve for voxel zero, identified by black and green dots) as well as the associated trade off that increases global SAR by 22% (increased area under the green curve compared to the black one).

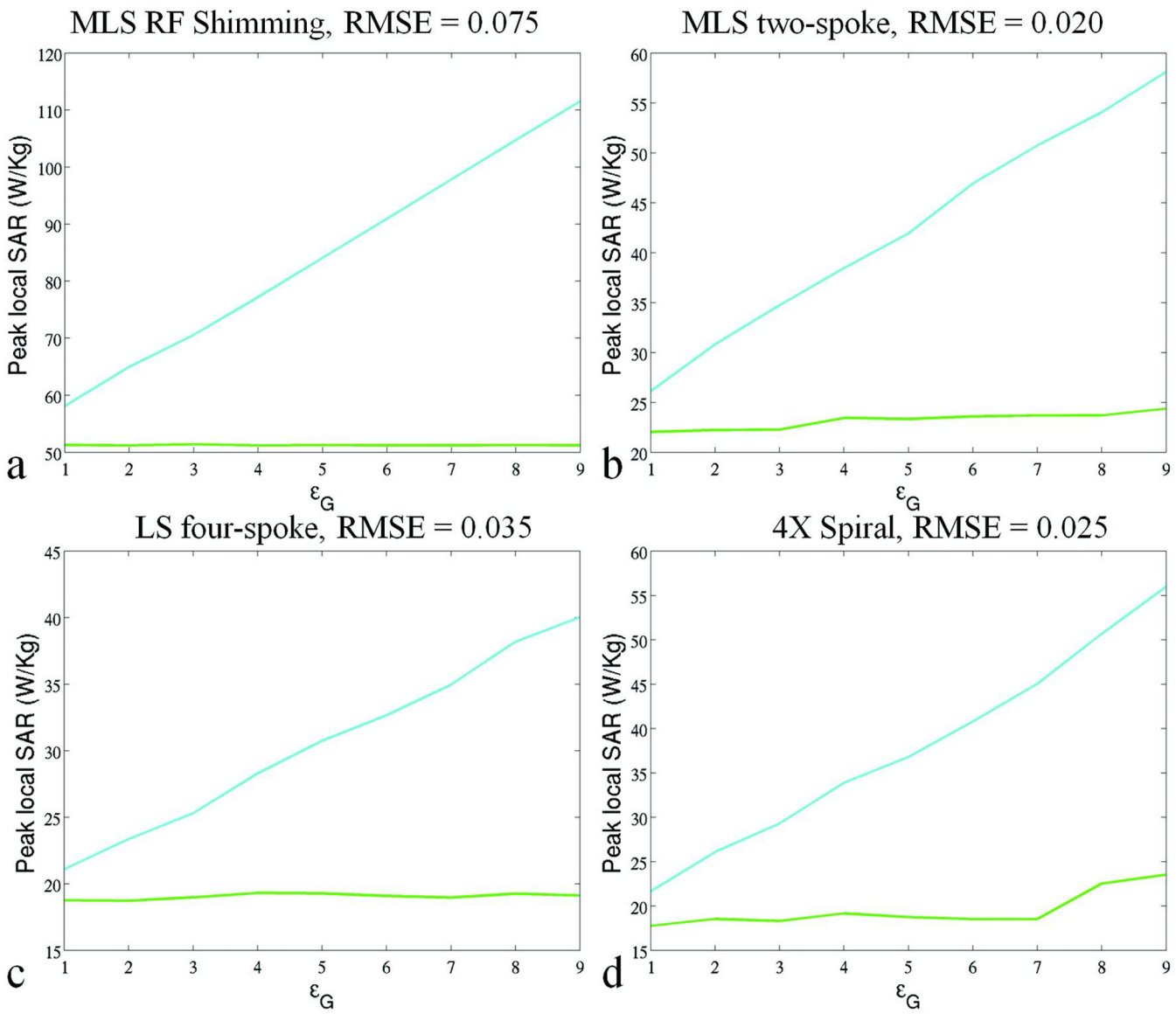

Figure 9.

Peak local SAR and its upper bound (Eq. [3]) as a function of overestimation factor, ε_G for four different pTx pulse designs. The graphs show the peak local SAR over the entire mode (green), its upper bound, which is the peak local SAR of the voxels in the subset, V_{sub}, determined by the model compression method plus the overestimation term (cyan). (a) RF shimming with MLS for RMSE = 0.075, (b) an MLS, two-spoke, slice-selective pTx excitation pulse with an MLS target criterion for RMSE = 0.02, (c) a four-spoke, slice-selective pTx excitation pulse with an LS target criterion for RMSE = 0.035, (d) and a 2D spiral-based excitation for a square box excitation with RMSE = 0.025.

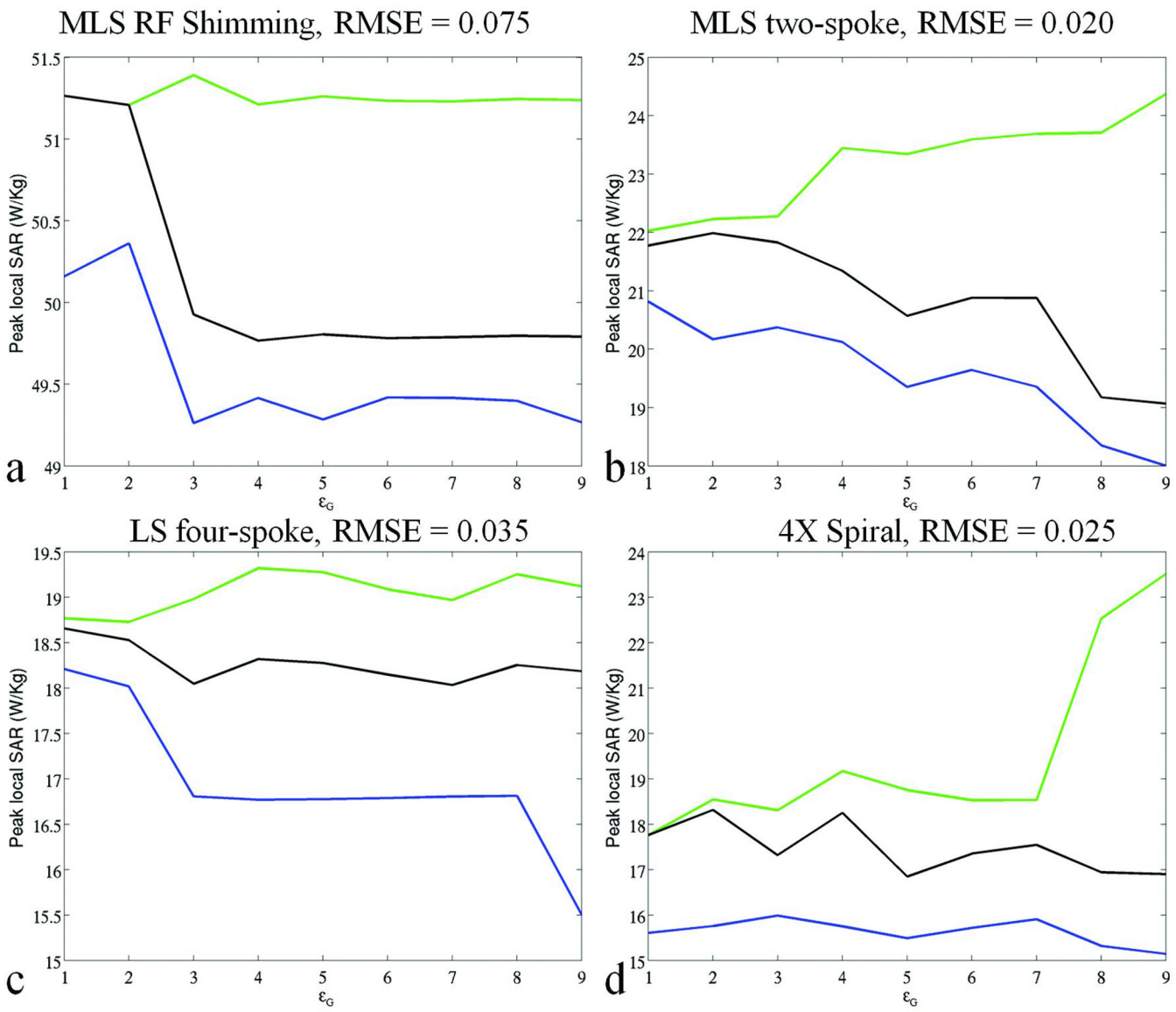

Figure 10.

Peak local SAR and its lower bounds as a function of overestimation factor, ε_G for four different pTx pulse designs. The graphs show the peak local SAR over the entire mode (green), the peak local SAR of the voxels in the subset, V_{sub}, determined by the model compression method without overestimation term (black), and the weighted local SAR of the voxels in the subset, V_{sub}, which is the PUPiL SAR (blue). (a) RF shimming with MLS for RMSE = 0.075, (b) an MLS, two-spoke, slice-selective pTx excitation pulse with an MLS target criterion for RMSE = 0.02, (c) a four-spoke, slice-selective pTx excitation pulse with an LS target criterion for RMSE = 0.035, (d) and a 2D spiral-based excitation for a square box excitation with RMSE = 0.025.